Disentangling Canted Phases and Phase Separation Regions with Spin Waves in Doped Manganites

José María Román (Univ. of Illinois)
Joan Soto (Univ. of Barcelona)

Outline

I. Continuum Double Exchange Model
- I.1 Doped Manganites Characteristics
- I.2 Continuum Double Exchange Model
- I.3 Effective Potential and Phase Diagram

II. Interaction with Spin Waves
- II.1 Goldstone Modes and Spin Waves
- II.2 Effective Lagrangian
- II.3 Spin Waves-Fermions Interaction

III. Spin Waves in Doped Manganites
- III.1 Heisenberg term Contribution
- III.2 Contribution from Conduction Fermions
- III.3 Dispersion Relation Parameters

IV. Canted Phases versus Phase Separation

V. Conclussions

I. Continuum Double Exchange Model

I.1. Manganites characteristics

general formulae $La_{1-x}A_xMnO_3$ (A-divalent)

Perovskite structure

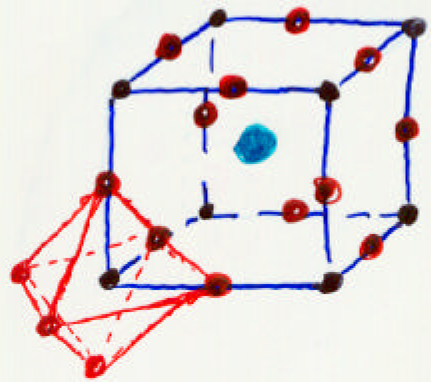

• Mn^{3+} ([Ar] $3d^4$)
Mn^{4+} ([Ar] $3d^3$)
• La^{3+}, Ca^{2+}, Sr^{2+}, Ba^{2+}
• O^{2-}

Electronic Structure

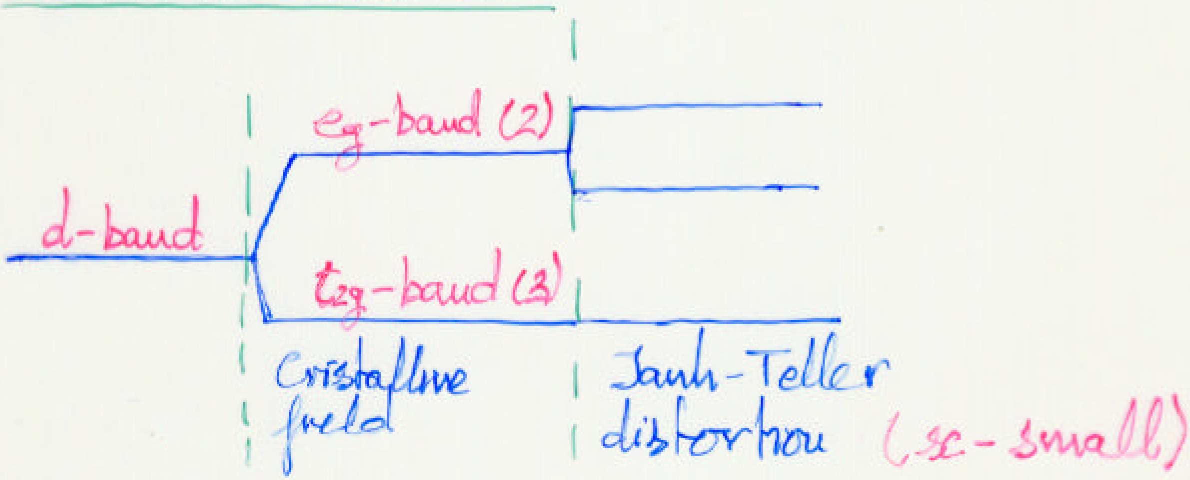

Magnetic Structure

$LaMnO_3$ $(x=0)$, $AMnO_3$ $(x=1)$ → AF, Semiconductor

$La_{1-x}A_xMnO_3$ $(0{,}2 < x < 0{,}4)$ → F, Conductor

Double Exchange Model

$Mn^{3+}(d^4)$ $\quad\quad$ $Mn^{4+}(d^3)$

Core classical spin $S=3/2$

The Hund interaction aligns the conduction electrons

Kondo problem with AF interaction

$$H = -t^{\ell} \sum_{\langle ij\rangle\sigma} c^{\dagger}_{i\sigma} c_{j\sigma} - J_H \sum_{i\sigma\sigma'} \vec{S}_i\, c^{\dagger}_{i\sigma} \frac{\vec{\sigma}_{\sigma\sigma'}}{2} c_{i\sigma'} + J^{\ell}_{AF} \sum_{\langle ij\rangle} \vec{S}_i \vec{S}_j$$

The hopping term produce
i) movement of conduction electrons
ii) change the sublattice

I.2. Continuum Double-Exchange Model (CDEM)

- CDEM describes low energy and long distance properties
- CDEM need fields slowly varying over the system

$\vec{M}_1(x), \Psi_1(x) \longrightarrow$ Sublattice 1

$\vec{M}_2(x), \Psi_2(x) \longrightarrow$ Sublattice 2

$$\begin{aligned}\mathcal{L}(x) = {} & \Psi_1^{\dagger}(x)\left[(1+i\epsilon)i\partial_t + \frac{\partial_i^2}{2m} + \mu + J_H \frac{\vec{\sigma}}{2}\vec{M}_1(x)\right]\Psi_1(x) + \\ & + \Psi_2^{\dagger}(x)\left[(1+i\epsilon)i\partial_t + \frac{\partial_i^2}{2m} + \mu + J_H \frac{\vec{\sigma}}{2}\vec{M}_2(x)\right]\Psi_2(x) + \\ & + t\left(\Psi_1^{\dagger}(x)\Psi_2(x) + \Psi_2^{\dagger}(x)\Psi_1(x)\right) - J_{AF}\vec{M}_1(x)\vec{M}_2(x)\end{aligned}$$

$t \sim z t^{\ell}$ $\qquad J_{AF} \sim \frac{z J_{AF}^{\ell}}{a^3}$

$J_H \sim J_H^{\ell}$

$$\frac{1}{2m} \sim a^2 t^{\ell} \sim z a t$$

$z = 6$ coordination

Energy levels of the CDEM

$$E = \frac{k^2}{2m} \pm \frac{|J_H|M}{2}\sqrt{1+\gamma^2 \pm 2\gamma\cos\frac{\theta}{2}} \qquad \gamma = \frac{2t}{J_H M}$$

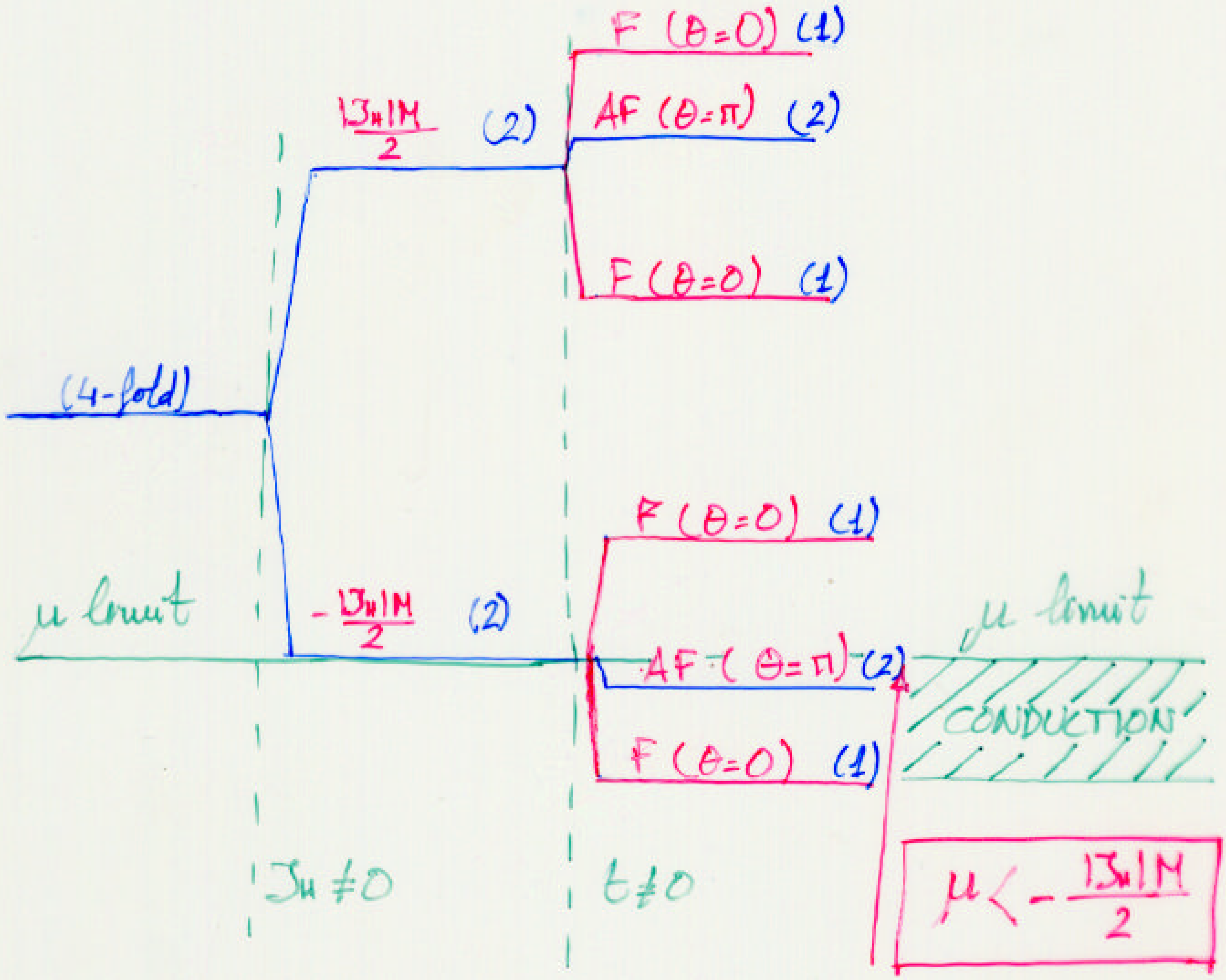

$$\mu = -\frac{|J_H|M}{2}\sqrt{1+\gamma^2-2\gamma\, y_0} \qquad y_0 < y_0^{max} = \frac{\gamma}{2}$$

I.3. Effective Potential and Phase Diagram

Integration of fermion fields in the path integral for constant configurations $\vec{M}_1, \vec{M}_2$

$$V_{eff} = J_{AF}\, \vec{M}_1 \cdot \vec{M}_2 + \frac{i}{VT} \operatorname{Tr} \log \hat{O}(\vec{M}_1, \vec{M}_2)$$

$$\hat{O}(\vec{M}_1, \vec{M}_2) = \begin{pmatrix} (1+i\varepsilon)\, i\partial_t + \frac{\partial_i^2}{2m} + \mu + J_H \frac{\vec{\sigma}}{2} \vec{M}_1 & t \\ t & (1+i\varepsilon)\, i\partial_t + \frac{\partial_i^2}{2m} + \mu + J_H \frac{\vec{\sigma}}{2} \vec{M}_2 \end{pmatrix}$$

The effective potential for $\gamma = \frac{2t}{J_H M} \ll 1$

$$V_{eff} = J_{AF} M^2 \left[(2y^2 - 1) - A \left((y_0 + y)^{5/2} \Theta(y_0 + y) + (y_0 - y)^{5/2} \Theta(y_0 - y) \right) \right]$$

$$y \equiv \cos\frac{\theta}{2} \qquad A \equiv \frac{z^{3/2}}{15\pi^2} \frac{t}{J_{AF} M^2 a^3}$$

Validity $\quad y_0 < y_0^{max} = \frac{\gamma}{2} \longrightarrow A > \frac{2 z^{1/2}}{15\pi^2} \frac{z |J_H| M}{2 (J_{AF} M^2 a^3)} y_0^{max}$

Phase diagram (y_0, A): Minimization respect "y"

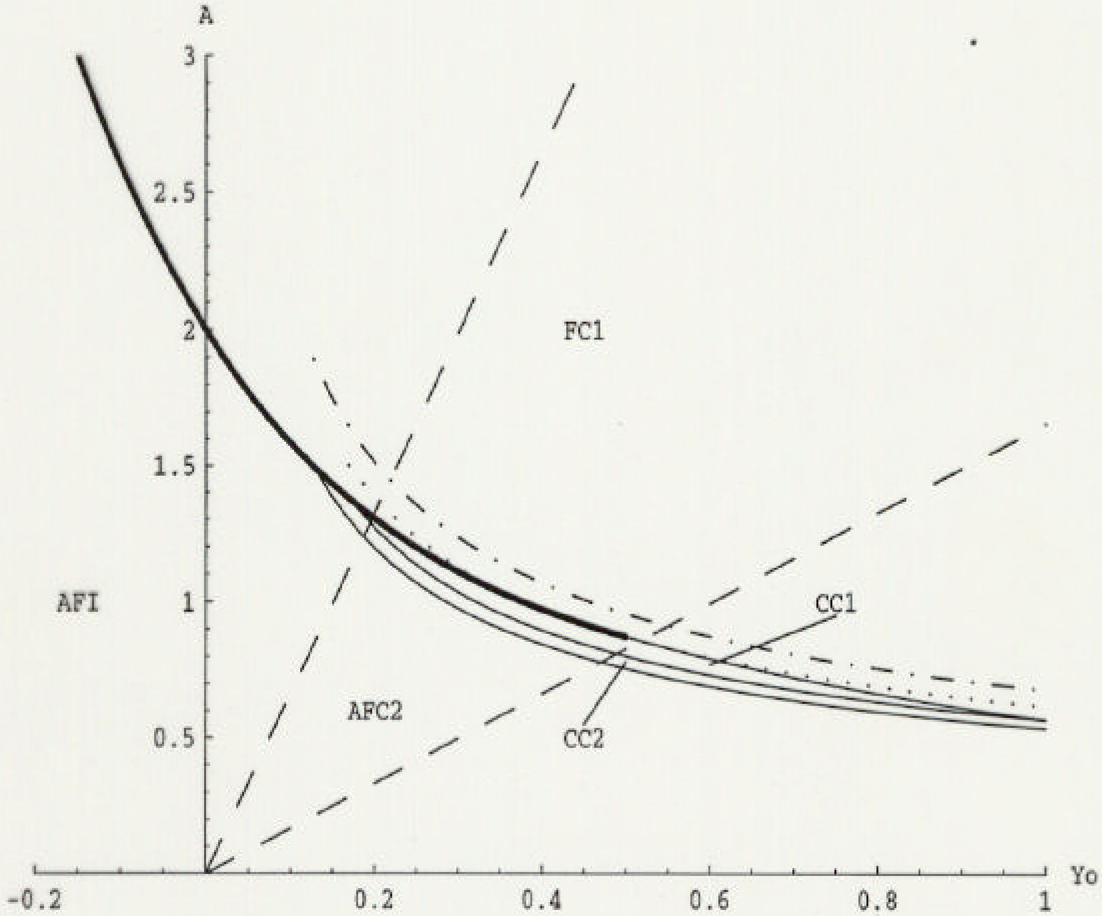

Figure 1: Phase diagram in the (y_0, A) plane. The thick solid line corresponds to first order transitions whereas the remaining solid lines to second order ones. The dotted and dashed dotted lines are the upper stability boundaries for the CC1 and CC2 phases respectively. The two dashed lines are the boundaries for the reliability of our model for $z|J_H|M/2(J_{AF}a^3M^2) \sim 50$ and $z|J_H|M/2(J_{AF}a^3M^2) \sim 200$ respectively. Only the part of the phase diagram to the left of the corresponding dashed line is trustworthy in each case.

$$x = -a^3 \frac{\partial V_{eff}}{\partial \mu} = -\frac{a^3}{t} \frac{\partial V_{eff}}{\partial y_0} .$$

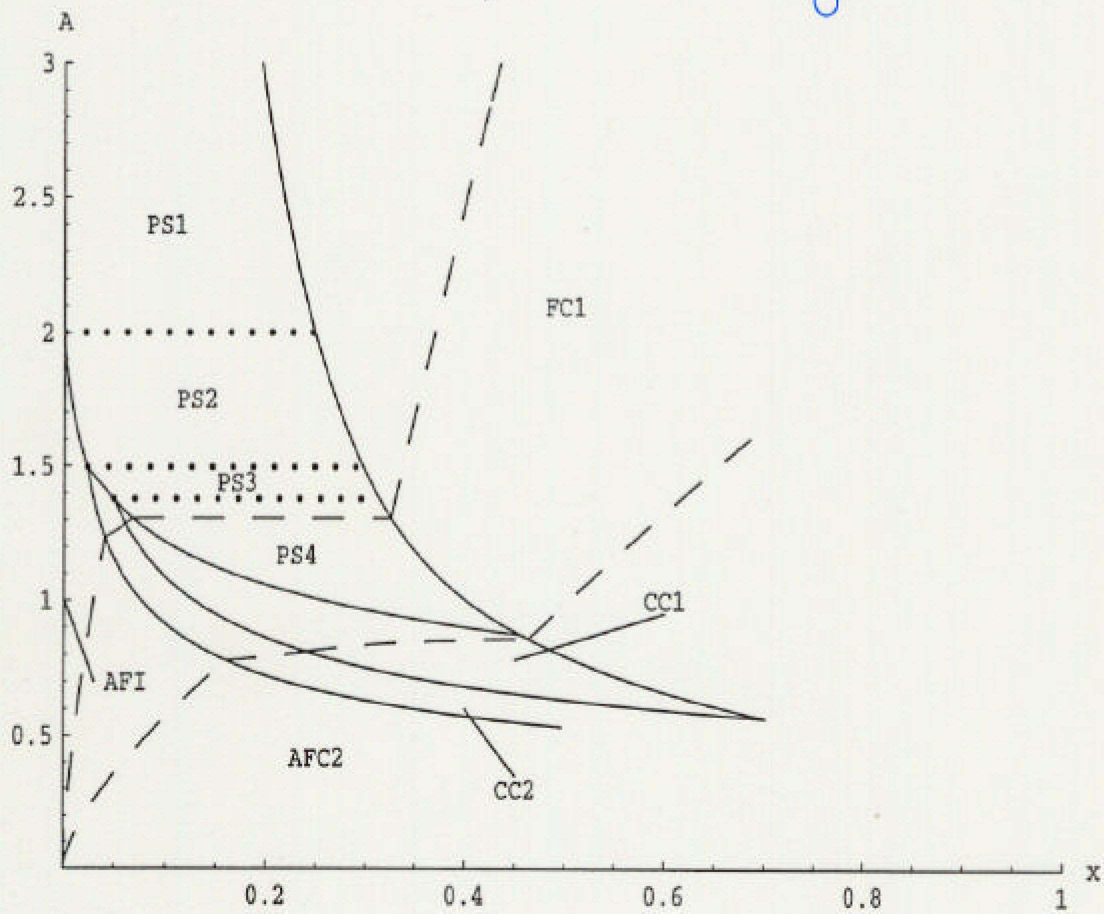

Figure 2: Phase diagram in the (x, A) plane. PSi $(i = 1, 2, 3, 4)$ indicates the new regions where the phases at their boundary may coexist. The $x = 0$ axis corresponds to the AFI phase. The two dashed lines are the boundaries for the reliability of our model for $z|J_H|M/2(J_{AF}a^3M^2) \sim 50$ and $z|J_H|M/2(J_{AF}a^3M^2) \sim 200$ respectively. Only the part of the phase diagram to the left of the corresponding dashed line is trustworthy in each case.

$$\frac{t}{J_{AF} a^3 M^2} \sim 10\text{-}20 \Longrightarrow \boxed{A \sim 1\text{-}2}$$

V. Conclussions

I. Continuum Double Exchange Model

- A simple model in the continuum was presented to describe the rich phase diagram for doped manganites

- Phase diagram presents

  AFI: Antiferromagnetic insulator
  AFC2: " conductor (2-bands)
  CC2: Canted " (2-bands)
  CC1: " " (1-band)
  FC1: Ferromagnetic " (1-band)
  PS: Phase Separation

- The canted phases are thermodynamically stable

II. Interaction with Spin Waves

- The effective lagrangian for the spin waves in the low energy and momentum regime

  F: One spin wave with quadratic D.R.
  AF: Two spin waves with linear D.R.
  C: One F and one AF spin waves

- Interaction lagrangian between the spin waves and the conduction fermions